JACS
JOURNAL OF THE AMERICAN CHEMICAL SOCIETY

Article

pubs.acs.org/JACS

Maximizing Synergistic Activity When Combining RNAi and Platinum-Based Anticancer Agents

Haihua Xiao,[†] Ruogu Qi,[†] Ting Li,[†] Samuel G. Awuah,[†,‡] Yaorong Zheng,[†,‡] Wei Wei,[§] Xiang Kang,[†] Haiqin Song,[†] Yongheng Wang,[†] Yingjie Yu,[†] Molly A. Bird,[†] Xiabin Jing,[⊥] Michael B. Yaffe,[†] Michael J. Birrer,[§] and P. Peter Ghoroghchian*[,†,∥]

[†]Koch Institute for Integrative Cancer Research, Massachusetts Institute of Technology, Cambridge, Massachusetts 02139, United States

[‡]Department of Chemistry, Massachusetts Institute of Technology, Cambridge, Massachusetts 02139, United States

[§]Department of Medicine, Massachusetts General Hospital, Harvard Medical School, Boston, Massachusetts 02114, United States

[⊥]State Key Laboratory of Polymer Physics and Chemistry, Changchun Institute of Applied Chemistry, Chinese Academy of Sciences, Changchun 130022, People's Republic of China

[∥]Dana-Farber Cancer Institute, Boston, Massachusetts 02115, United States

Supporting Information

ABSTRACT: RNAi approaches have been widely combined with platinum-based anticancer agents to elucidate cellular responses and to target gene products that mediate acquired resistance. Recent work has demonstrated that platination of siRNA prior to transfection may negatively influence RNAi efficiency based on the position and sequence of its guanosine nucleosides. Here, we used detailed spectroscopic characterization to demonstrate rapid formation of Pt-guanosine adducts within 30 min after coincubation of oxaliplatin [OxaPt(II)] or cisplatin [CisPt(II)] with either guanosine monophosphate or B-cell lymphoma 2 (BCL-2) siRNA. After 3 h of exposure to these platinum(II) agents, >50% of BCL-2 siRNA transcripts were platinated and unable to effectively suppress mRNA levels. Platinum-(IV) analogues [OxaPt(IV) or CisPt(IV)] did not form Pt-siRNA adducts but did display decreased in vitro uptake and reduced potency. To overcome these challenges, we utilized biodegradable methoxyl-poly(ethylene glycol)-*block*-poly(*ε*-caprolactone)-*block*-poly(L-lysine) (mPEG-*b*-PCL-*b*-PLL) to generate self-assembled micelles that covalently conjugated OxaPt(IV) and/or electrostatically complexed siRNA. We then compared multiple strategies by which to combine BCL-2 siRNA with either OxaPt(II) or OxaPt(IV). Overall, we determined that the concentrations of siRNA (nM) and platinum(II)-based anticancer agents (μM) that are typically used for in vitro experiments led to rapid Pt-siRNA adduct formation and ineffective RNAi. Coincorporation of BCL-2 siRNA and platinum(IV) analogues in a single micelle enabled maximal suppression of BCL-2 mRNA levels (to <10% of baseline), augmented the intracellular levels of platinum (by ∼4×) and the numbers of resultant Pt-DNA adducts (by >5×), increased the cellular fractions that underwent apoptosis (by ∼4×), and enhanced the in vitro antiproliferative activity of the corresponding platinum(II) agent (by 10−100×, depending on the cancer cell line). When combining RNAi and platinum-based anticancer agents, this generalizable strategy may be adopted to maximize synergy during screening or for therapeutic delivery.

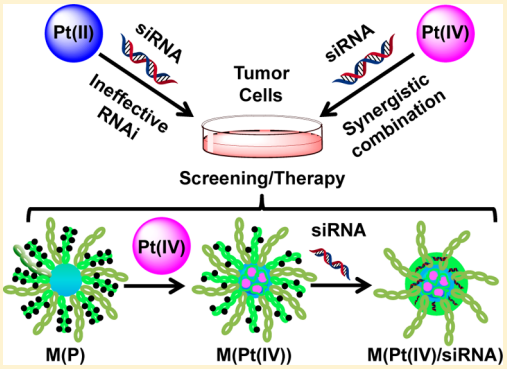

INTRODUCTION

Since the late 1970s, platinum(II)-based anticancer agents, including cisplatin and oxaliplatin, have become the most common class of chemotherapies used worldwide.[1,2] Whereas initial clinical response rates to platinum-containing regimens are high, the duration of activity in patients with metastatic cancers is generally short.[3,4] The various mechanisms by which these tumors develop resistance and acquire proliferative advantages are areas of very active investigation.[5−11] RNAi approaches have been used to screen for gene products that mediate these tumorigenic properties,[12−16] to validate putative drug targets,[17−19] and to develop therapeutic constructs.[20−22] Many of these experiments employ double-stranded small interfering RNAs (siRNAs) or microRNAs (miRNAs) that are synthesized with near-perfect complementarity to specific mRNA sequences. The siRNA (or miRNA) is delivered into the cell via a lipid or polymer-based transfection reagent, whereby it binds to the RNA-induced silencing complex (RISC) and leads to cleavage of its target mRNA.[23] The duration and level of mRNA knockdown are dependent on the cell type and the concentration of the siRNA that is delivered.[24]

Received: November 23, 2016
Published: February 6, 2017

DOI: 10.1021/jacs.6b12108
J. Am. Chem. Soc. 2017, 139, 3033−3044

Scheme 1. OxaPt(II) but not OxaPt(IV) Deactivates siRNA and a Strategy for Combining RNAi with an OxaPt(IV) Prodrug[a]

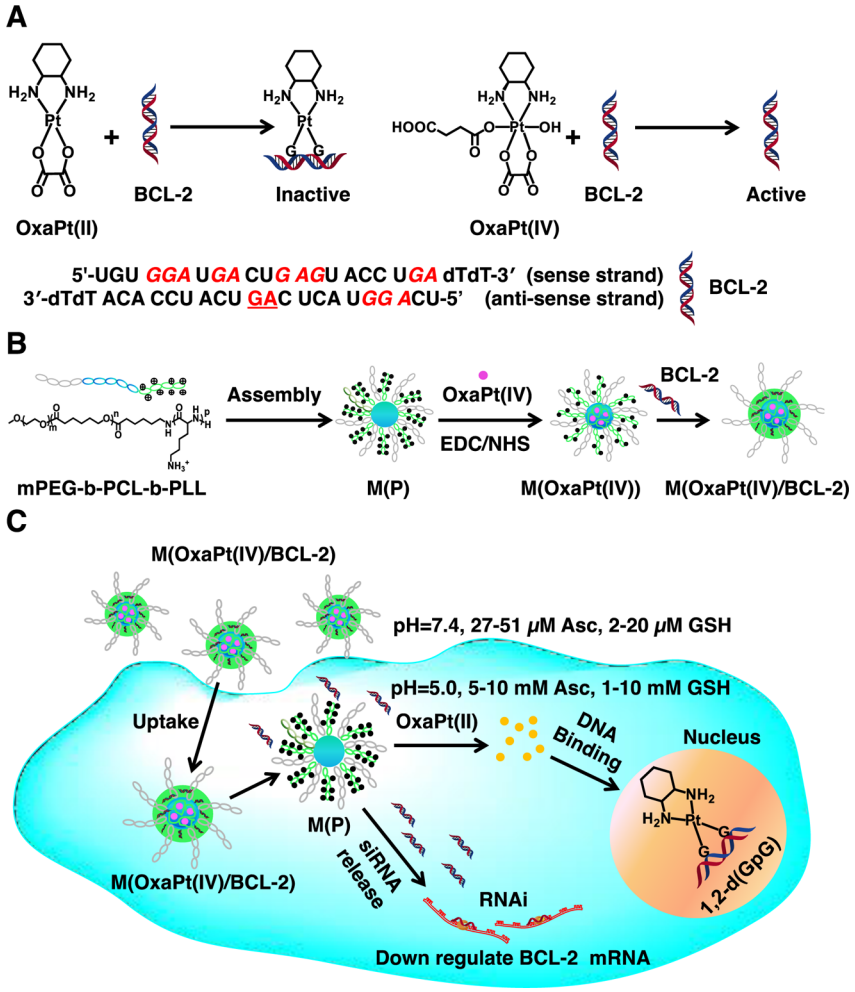

[a](A) Planar OxaPt(II) rapidly forms Pt-RNA adducts with BCL-2 siRNA, resulting in transcript inactivation; kinetically inert octahedral OxaPt(IV) species, however, do not. As predicted from the sequence of the BCL-2 siRNA, platination of a single GA region in the non-seed portion of the antisense strand (red/underlined) would be expected to affect silencing efficacy; the sense and anti-sense strands also contain other potential sites for further platination (red/italics). (B) Illustration of mPEG-*b*-PCL-*b*-PLL micelles (M(P)), incorporating OxaPt(IV) (M(OxaPt(IV)) or both OxaPt(IV) and BCL-2 siRNA in a single construct (M(OxaPt(IV)/BCL-2)); note, OxaPt(IV) is linked through an amide bond while BCL-2 siRNA is bound through electrostatic complexation to amino groups on the PLL chains of the micelles. (C) Intracellular uptake and the ultimate fate of M(OxaPt(IV)/BCL-2). The micelles are taken up by endocytosis, where high intracellular concentrations of ascorbic acid (Asc) and glutathione (GSH) rapidly convert OxaPt(IV) to OxaPt(II); free OxaPt(II) subsequently binds genomic DNA, resulting in Pt-DNA adduct formation. BCL-2 siRNA is liberated more slowly from the micelles, escaping from the endosome to down regulate BCL-2 mRNA expression in the cytoplasm.

When combining siRNA and platinum(II)-based anticancer agents, both species must be introduced into the cellular environment within a narrow temporal window in order to capture synergistic treatment effects.[12−19] The success of such endeavors relies implicitly on the assumption that the siRNA remains active, even for a few hours, when utilized in combination with platinum-based therapies.

It has long been appreciated that platinum(II)-based anticancer agents interact with DNA nucleobases, forming intra- and interstrand cross-links through the generation of adducts at the N7 positions of both guanine (G) and/or adenine (A).[25−27] The most commonly formed cross-links include d(pGpG) (i.e., the 1,2-guanosine-guanosine intrastrand cross-link) and d(pApG) (i.e., the 1,2-adenosine-guanosine intrastrand cross-link), which account for 47−50% and 23−28% of adducts, respectively.[25,28] With increasing quantities of intracellular Pt-DNA adducts, cell cycle arrest and eventually apoptosis ensue.[29−32] Given the base homology in RNA and DNA, recent investigations have sought to determine the presence, as well as to ascertain the biological consequences, of platinum-ribonucleic acid (Pt-RNA) adducts that may be similarly generated.

Cytoplasmic RNA is a major binding pool for platinum(II)-based anticancer agents; and, the concentrations of Pt-RNA adducts that are formed are ∼4−20 times greater than those of Pt-DNA adducts, following intracellular uptake of cisplatin.[33−35] Further, platinum(II)-containing agents readily form bidentate GG, GA/AG, and GXG (X ≠ G) adducts with siRNA and miRNA.[36,37] Whereas platination of neither the sense strand nor the seed portions of the antisense strand seems to interfere with silencing activity, Pt-RNA adducts that are formed in nonseed regions of the antisense strand induce thermal destabilization of the duplex of siRNA (or miRNA), which leads to decreased silencing of the complementary target mRNA.[36,37] The results of these investigations raise important questions as to whether the concentrations of siRNA and

DOI: 10.1021/jacs.6b12108
J. Am. Chem. Soc. 2017, 139, 3033−3044

platinum(II)-based anticancer agents that are administered in combination treatments are sufficient to form Pt-siRNA adducts in the cellular environment. siRNA inactivation through Pt-siRNA adduct formation could have implications for the results of numerous preclinical studies that have utilized such approaches either for discovery or for therapeutic intervention.[12−22] Moreover, different strategies by which to combine these two reactive species have not, hitherto, been rigorously compared.

Here, we sought to determine a generalizable method by which to combine RNAi and platinum-containing therapies in order to prevent premature siRNA inactivation and to maximize synergistic activity. We utilized oxaliplatin [OxaPt(II)] and cisplatin [CisPt(II)] as model platinum(II)-based anticancer agents. To advance our design, we also synthesized chemically inert platinum(IV) derivatives, denoted by OxaPt(IV) and CisPt(IV),[38−40] respectively (Schemes 1A, S1, and S2). Platinum(IV) analogues are activated by reduction to their corresponding platinum(II) species only after intracellular uptake within cancer cells, which contain supraphysiologic levels of glutathione and ascorbic acid (∼100 to ∼1000 fold excess over normal cells).[39,41−45] Employing platinum(IV)-containing agents offers an attractive means by which to overcome challenges associated with combining RNAi and platinum(II)-based therapies for discovery research and cancer treatment. The MCF-7 breast cancer and the OVCAR4 ovarian cancer cell lines were mainly employed as the in vitro model systems in our studies; and, the antiapoptosis protein B-cell lymphoma 2 (BCL-2) was selected as the target for RNAi. BCL-2 upregulation contributes to the development of acquired CisPt(II) resistance in various solid tumor malignancies.[5,46] Here, we used a BCL-2 siRNA that contained multiple GG and GA regions but only a single GA sequence outside of the seed portion of the antisense strand. Platination at this latter site was expected to result in maximal thermal destabilization with decreased mRNA silencing[36,37] (Scheme 1A). A micelle-based transfection reagent comprised of the triblock copolymer of methoxyl-poly(ethylene glycol)-*block*-poly(ε-caprolactone)-*block*-poly(L-lysine) (mPEG-*b*-PCL-*b*-PLL) was used to deliver OxaPt(IV) and/or siRNA (Scheme 1B). This vehicle was also employed to validate an optimal strategy for combining RNAi and platinum-based anticancer agents (Scheme 1C).

EXPERIMENTAL SECTION

Materials. mPEG-*b*-PCL-*b*-PLL was synthesized as previously described.[47] Its structure was verified by ^{1}H NMR spectroscopy and consisted of $mPEG_{114}$-*b*-PCL_{25}-*b*-PLL_{25}, where the subscript denotes the degree of polymerization of each individual monomer in a given block (Figure S1). This triblock copolymer is hereafter abbreviated "P". *N*-hydroxysuccinimide (NHS), 1-(3-dimethyl aminopropyl)-3-ethylcarbodiimide hydrochloride (EDC·HCl), guanosine 5′-monophosphate disodium salt (5′-GMP), and sodium ascorbate were purchased from Sigma-Aldrich. OxaPt(II) and CisPt(II) were purchased from ChemiChem International Development Co., Ltd. (Shenzhen, China). OxaPt(IV) analogues were synthesized and characterized by nuclear magnetic resonance (NMR) spectroscopy and mass spectrometry (MS), following procedures described below and in our previous studies[48] (Figures S2−S6). The CisPt(IV) derivatives were similarly synthesized and characterized as described.[38,40] All other chemicals and solvents were used without further purification. Control (c-) siRNA that targeted the sequence 5′-GGGUAAGUGUCCUACUGAAGU-3′, BCL-2 siRNA that targeted the sequence 5′-UGUGGAUGACUGAGUACCUGA-3′, and Alexa488-labeled BCL-2 siRNA (Alexa488 siRNA) were purchased from Integrated DNA Technologies (Coralville, Iowa); the c-siRNA did not match any known sequence in the human genome. Luciferase GL3 siRNA was purchased from GenePharma Co. Ltd. (Shanghai, China).

General Measurements. NMR, MS, graphite furnace atomic absorption spectroscopy (GFAAS), and UV−vis spectroscopy were used to study the reactions of various platinum species with either 5′-GMP or BCL-2 siRNA (see Supplemental Methods in the Supporting Information). In brief, ^{1}H, ^{13}C, and ^{195}Pt NMR spectra at RT were measured at 400, 100, and 86 MHz, respectively, using a Bruker NMR spectrometer (Bruker Corporation, Billerica, MA). MS measurements were performed on a Quattro Premier XE system equipped with an electrospray interface (ESI-MS; Waters, Milford, MA) as well as on a matrix-assisted laser-desorption ionization and time-of-flight MS (MALDI/TOF-MS) instrument (Bruker model MicroFlex). GFAAS and UV−vis measurements were conducted using an AAnalyst 600 GFAAS instrument (PerkinElmer, Waltham, MA) and an Infinite M200 Pro microplate reader (Tecan Systems, Inc., CA, USA), respectively. GFAAS was also used to determine the Pt content in all micelle formulations. Inductively coupled plasma MS (ICP-MS; ICP-MS 7900, Agilent Technologies, CA, USA) was used for quantitative determination of trace levels of Pt in cancer cells and to quantify the numbers of intracellular Pt-DNA adducts that were formed after treatment with various experimental groups.

Cell Culture. MCF-7 (human breast cancer), LUC^+ MCF-7 (luciferase expressing MCF7), OVCAR4 (human ovarian cancer), A2780 (CisPt(II)-sensitive), and A2780DDP (CisPt(II)-resistant) cell lines were obtained from ATCC and cultured at 37 °C, 5% CO_2 in Dulbecco's Modified Eagle Medium (DMEM, Gibco, Carlsbad, CA; MCF-7) or RPMI 1640 (LUC^+ MCF-7, OVCAR4, A2780, and A2780DDP) supplemented with 10% fetal bovine serum (FBS, Gibco).

Quantitative Reverse Transcription (RT-q)PCR. BCL-2 siRNA was first preincubated with platinum(II) or platinum(IV) species for various time periods and subsequently transfected into MCF-7 and OVCAR4 cells in 6-well plates, using an RNAiMAX Kit and by following the manufacturer's instructions (Invitrogen, Thermo-Fisher, USA). Briefly, 48 h after transfection, total RNA was isolated, using an RNeasy mini-kit (Qiagen, Germantown, MD), and quantified by NanoDrop (NanoDrop 2000, Thermo Scientific). A total of 300 ng of mRNA was subsequently subjected to RT-qPCR analysis, utilizing primers that targeted BCL-2 and glyceraldehyde 3-phosphate dehydrogenase (GAPDH), the SYBR Premix Ex (Clontech, Mountain View, CA), and an Applied Biosystems StepOne Real-Time PCR System (Thermo Scientific). Relative gene expression values were determined by the ΔΔCT method using StepOne Software v2.1 (Applied Biosystems, Foster City, CA). Data are presented as fold differences in mRNA expression for BCL-2 normalized to the housekeeping gene GAPDH and were obtained by employing a standard curve; results are reported relative to untreated (control) cells. The sequence of the primers used for BCL-2 and GAPDH are as follows: BCL-2 forward 5′-CTGCACCTGACGCCCTTCACC-3′; BCL-2 reverse 5′-CACATGACCCCACCGAACTCAAAGA-3′; GAPDH forward 5′-TTCACCACCATGGAGAAGGC-3′; and GAPDH reverse 5′-GGCATGGACTGTGGTCA TGA-3′ (Integrated DNA Technologies). The specificity of each set of primers was verified by melting curve analysis. Additional details may be found in Supplemental Methods in the Supporting Information.

Formation and Characterization of Polymeric Micelles. P-based micelles (M(P)) were prepared by an established nanoprecipitation method.[47] In brief, P (50 mg) was dissolved in DMF (10 mL); water (50 mL) was then added dropwise into the flask under continuous agitation, forming M(P) in suspension. The suspension was then dialyzed against water to remove the organic solvent and subsequently freeze-dried for storage. The critical micelle concentrations (CMCs) of M(P) and other micellar formulations (vide infra) were measured as previously reported,[49] using Nile red as the fluorescent probe. Particle sizes and zeta potentials were measured using a Nano ZS90 Zetasizer equipped with a vertically polarized He−Ne laser (Malvern Instruments, Malvern, PA). Images of various

DOI: 10.1021/jacs.6b12108
J. Am. Chem. Soc. 2017, 139, 3033−3044

micelle suspensions were obtained using a JEOL-1100 transmission electron microscope (JEOL USA, Peabody, MA).

Conjugation of OxaPt(IV) to M(P). EDC/NHS chemistry was employed to conjugate OxaPt(IV) to P via an amide bond. Briefly, EDC·HCl (0.191 g, 1 mmol) and NHS (0.115 g, 1 mmol) were dissolved in deionized H_2O under stirring. OxaPt(IV) (0.42 g, 0.8 mmol) was then added to the solution. After the suspension mixture became clear, P (0.5 g; containing 1.25 mmol NH_2 groups) was added to the reaction mixture (100 mL) and stirred at RT for 24 h; the suspension was then dialyzed against water for an additional 12 h and lyophilized to isolate OxaPt(IV)-conjugated micelles (M(OxaPt(IV))). The Pt content of the micelles was measured by GFAAS.

Complexation of siRNA with Polymeric Micelles. Suspensions of M(P) or M(OxaPt(IV)) were diluted with Opti-MEM media (Invitrogen) to different concentrations, varying the final numbers of amino groups in solution. Equal volume solutions containing BCL-2 or c-siRNA where then added to the micelles, varying the initial ratios of free amines to phosphates (N/P) in suspension. siRNA-complexed micelles were then formed by gentle pipetting and allowed to equilibrate for 30 min at RT. For electrophoresis-retardation analyses, complexes formed from either M(P) or M(OxaPt(IV)) and siRNA at different initial N/P ratios, ranging from 0 to 4, were prepared for a fixed concentration of siRNA (1 mM). The samples were run on a 1% agarose gel in 0.5 mM tris-borate-EDTA buffer (TBE buffer; 89 mM Tris, 90 mM boric acid, 2 mM EDTA, pH 8.3) at 80 V and for 30 min. Bands containing free and micellar-bound siRNA were visualized using a UV illuminator (Tanon 3000, Biotanon, Shanghai, China) after ethidium bromide staining.

To determine the maximal loading of siRNA and the efficiency of micellar complexation, Alexa488-labeled BCL-2 siRNA was complexed with M(P) or M(OxaPt(IV)) at different initial N/P ratios, varying from 0 to 16, and subsequently quantified by both UV−vis and fluorescence spectroscopy. To determine the amounts of micellar-complexed siRNA necessary for effective RNAi, Luciferase GL3 siRNA was complexed with M(P) or M(OxaPt(IV)) at an initial N/P ratio of 8; and, the percentage of initial luciferase mRNA expression (relative to controls) was quantified as a function of different concentrations of Luciferase GL3 siRNA that were used for transfection, ranging from 25 to 150 nM. Detailed information on micelle preparation and various siRNA-complexed formulations may be found in Supplemental Methods in the Supporting Information.

Intracellular Uptake of Fluorophore-Labeled Micelles. For confocal microscopy experiments, MCF-7 and OVCAR4 cells were plated on coverslips in 6-well plates (4×10^5 cells/well) and cultured with RPMI 1640 supplemented with 10% FBS for 24 h. The cells were then incubated either for 30 min or for 4 h with micelles that were electrostatically complexed with Alexa488-labeled BCL-2 siRNA (50 nM) and that were covalently conjugated to Cy5.5 with and without OxaPt(IV), forming M(Cy5.5/Alexa488 siRNA) and M(Cy5.5/Alexa488 siRNA/OxaPt(IV)), respectively. After removal of the media, the cells were then washed twice with cold phosphate buffered saline (PBS, pH 7.4, 0.01 M) and fixed with 4% formaldehyde (Sigma-Aldrich, St. Louis, USA). To label the cell nuclei, samples were incubated with 1 μL of DAPI (1 mg/mL; Sigma-Aldrich, St. Louis, USA) for 15 min in PBS and were subsequently rinsed extensively with PBS. Slides were mounted on coverslips and imaged, using a confocal laser scanning microscopy system (Olympus FV1000, Olympus Corporation, Bridgeport, CT).

For flow cytometry measurements, MCF-7 and OVAR4 cells were similarly cultured in 6-well plates (4×10^5 cells/well) prior to incubation with M(Cy5.5/Alexa488 siRNA) or M(Cy5.5/Alexa488 siRNA/OxaPt(IV)) either for 30 min or for 4 h. The cells were washed twice with cold PBS, lysed with trypsin−EDTA solution, collected by centrifugation (1500 rpm, 5 min), and, finally, analyzed for fluorescence content, using a FACSCalibur flow cytometer (BD Biosciences, San Jose, CA). Cells with fluorescence above the threshold intensity for untreated cells (i.e., blank) were quantified and compared. The percentage of these cells in the total population was considered as a measure of uptake efficiency. Data were analyzed using FlowJo software Version 7.6.2 (Tree Star, Ashland, OR).

Quantification of Intracellular Uptake of Platinum Species. MCF-7 cells were seeded in 12-well plates (1×10^5 cells/well) and incubated overnight in DMEM containing 10% FBS (1 mL). Various platinum-containing agents (OxaPt(II), OxaPt(II) + M(c-siRNA), OxaPt(II) + M(BCL-2), M(OxaPt(IV)/c-siRNA), or M(OxaPt(IV)/BCL-2)) were then added to each well (100 μL aliquots and to final Pt concentration of 10 μM). For siRNA-containing treatments, the final siRNA concentration in each well was 100 nM. After either 1 or 4 h of incubation, media were removed and the cells were thoroughly washed ×5 with cold PBS. The cells were then lysed with nitric acid prior to ICP-MS measurements. For quantification of Pt-DNA adducts, cells were similarly incubated with each platinum-containing agent but for 24 h. The cells were then washed and the DNA was extracted using a Genome DNA extraction kit, following the manufacturer's instructions (Thermo Scientific, USA). DNA concentrations were determined by NanoDrop, and the quantity of DNA-bound Pt was determined by ICP-MS.

In Vitro Cytotoxicity. MCF-7, OVCAR4, A2780, and A2780DDP cells were seeded in 96-well plates (5×10^3 cells/well). DMEM (MCF-7; 100 μL) or RPMI-1640 (OVCAR4, A2780, A2780DDP; 100 μL) supplemented with 10% FBS was added to each well. The cells were then incubated at 37 °C for 24 h prior to the addition of OxaPt(II), OxaPt(IV), or M(OxaPt(IV)) with or without micellar-complexed BCL-2 or c-siRNA. For siRNA-containing treatments, an equivalent concentration of siRNA (100 nM) was added to each well. The cells were subsequently allowed to incubate at 37 °C for 72 h prior to evaluation of cellular viability, using the colorimetric MTT assay. In brief, MTT reagent in PBS buffer (5 mg/mL; 20 μL) was added to each well and allowed to incubate for 4 h. DMSO (150 μL) was then added to replace the MTT-containing media. After gentle agitation (5 min), the absorbance of each well at 570 nm was recorded on a Bio-Rad Plate Reader (Hercules, CA). ABS at 650 nm was set as background and used for subtraction. All experiments were conducted in triplicate.

Cellular Apoptosis Assays. MCF-7 cells were cultured in 6-well plates (5×10^5 cells/well) and incubated with various treatments at a fixed Pt concentration (20 μM). After 36 h, apoptotic cells were detected by flow cytometry, using the Annexin V-FITC Apoptosis Detection Kit I (BD Biosciences, San Jose, CA); the results were analyzed using FlowJo software Version 7.6.2.

RESULTS AND DISCUSSION

Monitoring the Reaction of siRNA with Various Platinum-Based Species. OxaPt(II) and CisPt(II) bind preferentially to guanine and adenine bases in both DNA and RNA.[25−27,33−35] To compare the relative reactivity of OxaPt-(IV) and CisPt(IV) to their platinum(II) counterparts, we first incubated each compound for different time intervals with 5′-GMP (i.e., 30 min, 1 h, 3 h, 6 h or 12 h) and in conditions that would mimic a typical in vitro RNAi experiment (i.e., coincubation of the two species at 37 °C). Formation of Pt-$(5'\text{-GMP})_2$ adducts was readily detectable by ESI-MS when 5′-GMP was incubated with OxaPt(II) but not with OxaPt(IV) (Figures 1A, 1B and S7). These findings were further confirmed by MALDI/TOF-MS measurements of the same suspensions, showing that Pt-$(5'\text{-GMP})_2$ adducts were detected within 1 h in solutions containing OxaPt(II) or CisPt(II) but not OxaPt(IV) or CisPt(IV) (Figures S8 and S9). To further quantify differences in the kinetics of Pt-$(5'\text{-GMP})_2$ adduct formation, ^{1}H NMR spectra were obtained for 5′-GMP solutions at various time intervals after the addition of different platinum-(II) or platinum(IV) species and under identical conditions. The chemical shifts of the H8 proton on the guanosine base (8.5 ppm in the (diamino-1,2-cyclohexane)-Pt$(5'\text{-GMP})_2$, DACHPt$(5'\text{-GMP})_2$) adduct vs 8.09 ppm in unreacted 5′-GMP) were monitored at several time points after coincubation of 5′-GMP (10 mM) with either OxaPt(II) or OxaPt(IV) (5

DOI: 10.1021/jacs.6b12108
J. Am. Chem. Soc. 2017, 139, 3033−3044

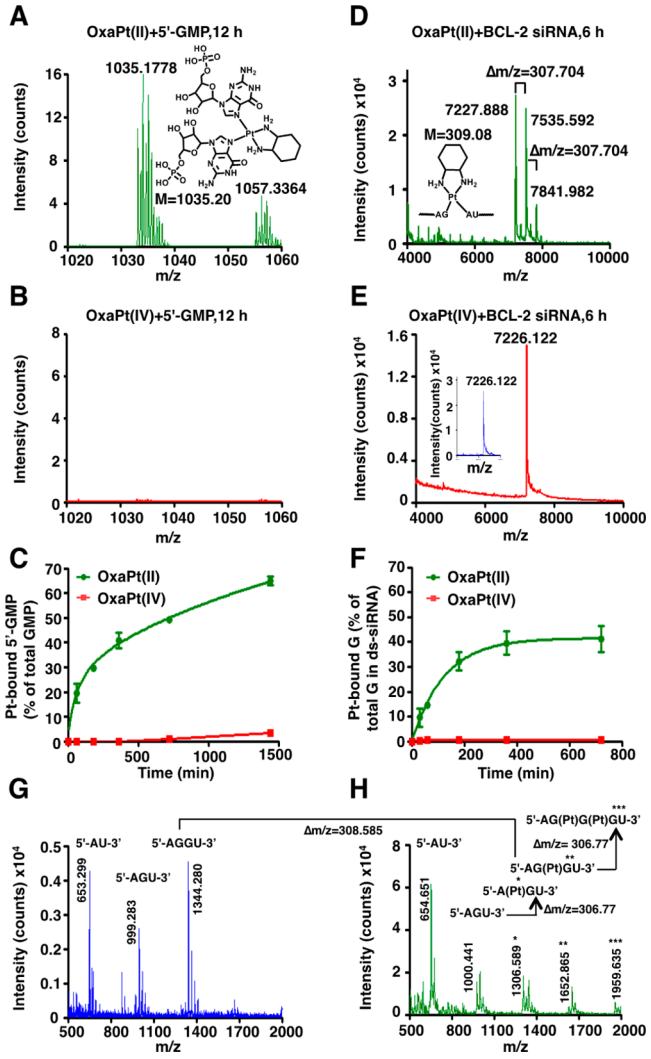

Figure 1. OxaPt(II) rapidly binds 5′-GMP as well as siRNA, forming Pt-RNA adducts, while OxaPt(IV) does not. Representative ESI-MS spectra of solutions of 5′-GMP (10 mM) at 12 h after incubation with either (A) OxaPt(II) (5 mM) or (B) OxaPt(IV) (5 mM) at 37 °C. The presence of the DACHPt(5′-GMP)$_2$ adduct was monitored over time by measuring changes in the relative height of the peak at m/z = 1035.2; the structure and molecular weight of bis-adducts are shown in A, inset. Note: other peaks in the ESI spectra correspond to adducts formed with Na^+ and K^+; see also Figure S7 (Supporting Information) for spectra at other time points. (C) Kinetics of the binding of various Pt-based agents to 5′-GMP; results are depicted as the molar percentage of the total 5′-GMP pool in solution and were determined by ^{1}H NMR spectroscopy. Representative MALDI/TOF-MS spectra of the products formed after 6 h of incubation of BCL-2 ss-siRNA (50 μM) with either (D) OxaPt(II) (500 μM) or (E) OxaPt(IV) (500 μM) at 37 °C. The spectrum of unreacted ss-siRNA is shown in E, inset. (F) Binding kinetics of OxaPt(II) and OxaPt(IV) (50 μM) to BCL-2 ds-siRNA (5 μM) as measured by GFAAS. Data are expressed as the percentage of platinum-bound G nucleotides within the ds-siRNA suspension. MALDI/TOF-MS was also conducted after enzymatic cleavage of the antisense strand of BCL-2 siRNA (50 μM) by RNase A either (G) before or (H) after incubation with OxaPt(II) (500 μM) to demonstrate sites of platination. 5′-AC-3′, 5′-AGU-3′, and 5′-AGGU-3′ are the cleavage products of the native BCL-2 ss-siRNA. Platination of the G and/or A sites in the BCL-2 ss-siRNA resulted in the addition of one or more DACHPt moieties, yielding 5′-A(Pt)GU-3′(*), 5′-A(Pt)GGU-3′(**), and 5′-A(Pt)G-(Pt)GU-3′(**); note, here Pt denotes DACHPt.

mM) (Figure S10). By integrating the ratio of the two peaks at each time point, the relative amounts of Pt-bound 5′-GMP to free 5′-GMP were determined in solutions containing OxaPt-(II) (green) or OxaPt(IV) (red) and plotted as a function of time (Figure 1C). The results showed that approximately 10% of the 5′-GMP pool consisted of DACHPt(5′-GMP)$_2$ adducts after 30 min of incubation with OxaPt(II), that the number of adducts that were formed increased over the first 6 h, reaching 40% of the total pool, and that they continued to increase over time. Similar early formation and time dependent increases in the numbers of Pt(NH$_3$)$_2$(5′-GMP)$_2$ adducts were seen when 5′-GMP was incubated with CisPt(II) but not with CisPt(IV) (Figure S11). Taken together, these model reactions of 5′-GMP with various platinum species support a rationale for combining RNAi approaches with platinum(IV)- as opposed to platinum(II)-based anticancer agents, which would otherwise react with similar nucleosides in RNA macromolecules and which would lead to inactivation of the siRNA or miRNA species.

We next sought to ascertain the kinetics of Pt-siRNA adduct formation by using the antisense strand of BCL-2 siRNA. This single-stranded (ss-)siRNA (50 μM) was incubated with different platinum(II)- and platinum(IV)-based anticancer agents (500 μM), which were present in a 10-fold excess in order to account for the relative concentrations of RNA to platinum species that are typically employed in RNAi and cytotoxicity experiments, respectively.[12−19] MALDI/TOF-MS spectra were taken at various time points after their coincubation at 37 °C. These experiments demonstrated that Pt-siRNA adducts could be detected as early as 1 h after the incubation of ss-siRNA with OxaPt(II) (Figures 1D and S12). Three major peaks were detected and attributed to unreacted BCL-2 ss-siRNA (m/z = 7227.888), BCL-2 ss-siRNA with one DACHPt^{2+} adduct (m/z = 7535.592), and BCL-2 ss-siRNA with two DACHPt^{2+} adducts (m/z = 7841.982). Note, the molecular weight of DACHPt was 309.08 and the $\Delta m/z$ of ss-siRNA upon formation of the siRNA-DACHPt^{2+} mono adduct was 307.704; ss-siRNA lost two H^+ after binding with OxaPt(II) and added another H^+, keeping it at the +1 charge state. The unmodified BCL-2 ss-siRNA had a molecular weight of 7224.401 and displayed a +1 charged mass peak at m/z = 7226.122 (Figure 1E, inset). The margin of error for the MALDI/TOF-MS was ±0.1%; thus, for free ss-siRNA a variation of 0.722 Da units was within the range of precision for the MALDI/TOF-MS instrument. Compared to OxaPt(II), CisPt(II) is known to undergo more facile aquation of its planar ligands, decreasing its relative stability and increasing its reactivity toward ss-siRNA. When BCL-2 ss-siRNA was incubated with CisPt(II), numerous Pt-siRNA adducts were detected as early as 30 min after CisPt(II) addition (Figure S13). Notably, no Pt-siRNA adducts were detected in solutions of BCL-2 ss-siRNA containing either OxaPt(IV) or CisPt(IV) and even after 24 h of coincubation under similar conditions (37 °C; Figure 1E, S12 and S13).

GFAAS measurements of ds-siRNA that had been isolated after coincubation with various platinum species were also conducted to quantify the amounts of siRNA-bound Pt over time. These results indicate that a total of ∼4 Pt atoms bound to ds-siRNA within 3−6 h after incubation with OxaPt(II) (Figure S14), which corresponded to platination of ∼40% of the G nucleotides of the ds-siRNA (Figure 1F). Notably, no Pt was detected by GFAAS even in ds-siRNA solutions that had been incubated with OxaPt(IV) for up to 12 h. These results

DOI: 10.1021/jacs.6b12108
J. Am. Chem. Soc. 2017, 139, 3033−3044

Table 1. Summary of Different ds-RNA Macromolecules, Various Platinum-Containing Anticancer Agents, Their Reaction Rate Constants ($k_{2,app}$), and the Percentages of ds-siRNA That Are Expected to Be Deactivated Due to Platination as a Function of Reaction Time and Initial Concentration of the Platinum-Containing Species

							% ds-siRNA Deactivated Due to Platination (i.e., % ss-siRNA)									
							30 min		1 h		3 h		6 h		24 h	
Ref	RNA	Length	# Gs	Species	$k_{2,app}$ ($M^{-1}s^{-1}$)	Std Dev	1 μM	10 μM	1 μM	10 μM	1 μM	10 μM	1 μM	10 μM	1 μM	10 μM
37a	RNA-1	15	6	CisPt(II)	22.1	1.7	3.9	33	7.6	55	21	91	38	99	85	100
	RNA-2	15	6	CisPt(II)	20.1	1.1	3.6	30	7.0	52	20	89	35	99	82	100
	miR-146a	21	9	CisPt(II)	20.4	0.6	3.6	31	7.1	52	20	89	36	99	83	100
37b	RNA-1	15	6	CisPt(II)	7.7	0.5	1.4	13	2.7	24	8.0	57	15	81	49	100
	RNA-1−1-S	13	5	CisPt(II)	10.5	0.6	1.9	17	3.7	32	11	68	20	90	60	100
	RNA-1−2	13	6	CisPt(II)	23.6	1.0	4.2	35	8.1	57	23	92	40	99	87	100
	RNA-1−3	15/16	6	CisPt(II)	29.7	1.1	5.2	41	10	65	27	96	47	100	92	100
	RNA-1−4	17	6	CisPt(II)	>30.0	N/A	5.3	42	10	66	27	96	48	100	93	100
this work	BCL-2 siRNA	20	10	CisPt(II)	12.7	1.2	2.3	20	4.5	37	13	75	24	94	67	100
				OxaPt(II)	5.3	2.3	0.9	9	1.9	17	5.6	44	11	68	37	99
				CisPt(IV)	3.0	1.2	0.5	5	1.1	10	3.2	28	6.2	47	23	92
				OxaPt(IV)	0.2	N/A	0.0	0.4	0.1	0.7	0.2	2.2	0.4	4.3	1.7	16

were further corroborated by UV−vis measurements of the time-dependent platination of ds-siRNA, which has been shown to convert it to ss-siRNA, via monitoring of the hyperchromic (i.e., ΔA-value at λ = 260 nm) and bathochromic shifts (from a maximum at λ ca. 258 nm to a maximum at λ ca. 260 nm) that follow nucleic acid duplex melting.[37b] By first varying the initial concentrations of ds-siRNA (from 0.5 to 2 μM) for a fixed and excess (>10-fold) amount of CisPt(II) (20 μM), we verified that ss-siRNA was generated via a pseudo-first order reaction and that the apparent second-order rate constant ($k_{2,app}$) could be derived from the linear relationship between the observed rate constant (k_{obs}) and the initial concentration of the platinum species (see Figure S15 and Table S1):

$$[\text{ss-siRNA}]_t = [\text{ds-siRNA}]_o \times (1 - e^{(-k_{obs}t)})$$

$$k_{2,app} = k_{obs}/[\text{platinum species}]_o$$

UV−vis spectroscopy was similarly used to observe the reactions of other platinum species with ds-siRNA, verifying that the $k_{2,app}$ for OxaPt(II), CisPt(IV), and OxaPt(IV) were approximately 40%, 25% and 2% that of CisPt(II) (Table 1). Moreover, when ds-siRNA was incubated with CisPt(II) at concentrations that are typically employed for in vitro cytotoxicity experiments (i.e., >10 μM), approximately 50% of the ds-siRNA transcripts were converted to ss-siRNA by 1−3 h. Notably, other investigators have previously measured higher reaction rate constants for CisPt(II) with ds-RNA, whereby similar results would be expected in less than 1 h of coincubation (Table 1 and refs 33−35). Given the decreased reactivity of OxaPt(II) when compared to CisPt(II), analogous levels of ds-siRNA deactivation (from conversion to ss-siRNA via platination under identical reaction conditions) could be expected between 3 and 6 h of coincubation. Notably, as both CisPt(IV) and OxaPt(IV) were even less active than OxaPt(II), neither significant ds-siRNA platination nor deactivation were expected to proceed in their presence and under identical in vitro reaction conditions.

To determine the exact sites of platination on a nucleic acid transcript, we next conducted MALDI/TOF-MS experiments using a model ss-oligonucleotide of DNA that contained a single GG site, verifying the formation of mono- and bis-Pt-DNA adducts in the presence of OxaPt(II) but not OxaPt(IV) (Figure S16). MALDI/TOF-MS was then performed after enzymatic cleavage of the antisense strand of BCL-2 siRNA by RNase A, either before (Figure 1G) or after incubation with OxaPt(II). These experiments demonstrated two distinct sites on the ss-siRNA transcript that were platinated with either one or two DACHPt moieties, including the 5′-AGGU-3′ segment in the seed portion and the 5′-AGU-3′ site in the nonseed portion of the antisense strand (Figures 1H and S17).

Platination of the nonseed portion of the antisense strand was expected to affect RNAi efficacy.[36,37] To test this hypothesis, we studied changes in the relative silencing activity of BCL-2 ds-siRNA that was preincubated with different platinum(II) and platinum(IV) agents prior to cellular exposure. Using a fixed concentration of siRNA (7.5 nM), different concentrations of platinum-based species (either 0.75 or 7.5 μM), and various incubation times (ranging from 30 min to 24 h), we effectively varied the numbers of Pt-siRNA adducts that were present on the siRNA transcript prior to transfection. The siRNA was subsequently diluted (to a final concentration of 1.5 nM) and combined with the commercially available transfection reagent Lipofectamine (RNAiMAX) for delivery to both MCF-7 and OVCAR4 cells. RT-qPCR of BCL-2 mRNA isolated from these cells at 48 h after transfection showed ineffective BCL-2 silencing (i.e., greater than 30% of baseline mRNA expression) by siRNA (1.5 nM) that had been preincubated with a 1000-fold excess of OxaPt(II) for >3 h (Figure 2 and S18). CisPt(II) was more reactive than OxaPt(II) and ineffective BCL-2 mRNA suppression was seen even after 30 min of coincubation of BCL-2 siRNA with CisPt(II) under identical conditions. The activity of the siRNA was unperturbed by >24 h of exposure to similar concentrations of either OxaPt(IV) or CisPt(IV). Note, both the concentrations and the relative ratios of siRNA to platinum-based species that were used for these studies were typical of those employed for in vitro RNAi and cytotoxicity experiments, respectively.[12−19] Taken together, these experiments support a generalizable phenomenon whereby siRNA rapidly reacts with platinum(II) species that are present at >1 μM concentrations, leading to irreversible Pt-siRNA adduct formation and ineffective RNAi within as little as 1−3 h of coincubation. These results further highlight the value of combining RNAi approaches with

DOI: 10.1021/jacs.6b12108
J. Am. Chem. Soc. 2017, 139, 3033−3044

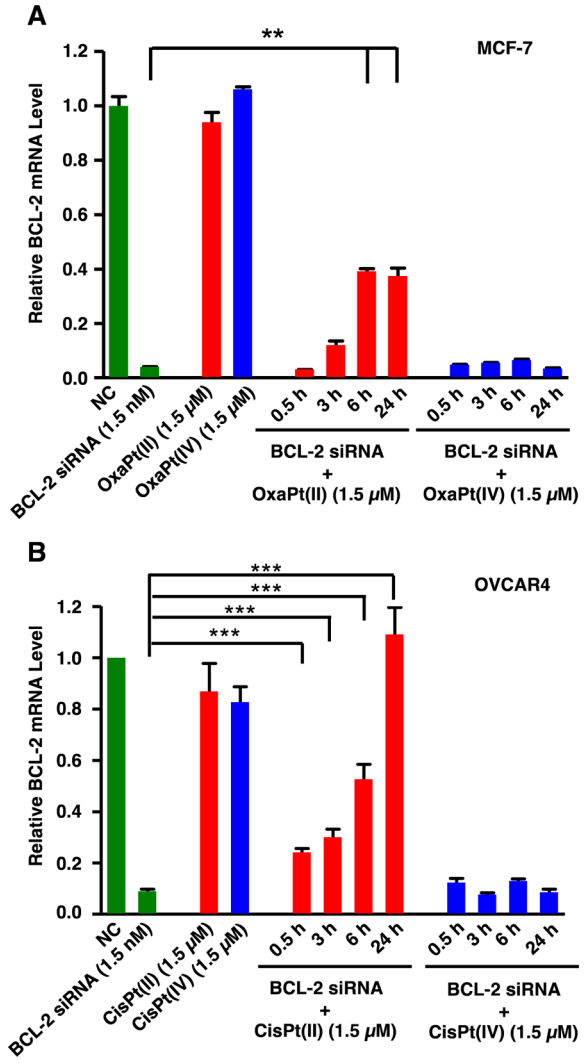

Figure 2. Incubation of siRNA with OxaPt(II) or CisPt(II) results in a time-dependent decrease in RNAi efficacy. Relative BCL-2 mRNA levels in (A) MCF-7 breast cancer cells and (B) OVCAR4 ovarian cancer cells at 37 °C and at 48 h after Lipofectamine-based transfection of BCL-2 siRNA. BCL-2 siRNA (1.5 nM) was utilized directly or was first preincubated with either different platinum(II)-based anticancer agents (i.e., OxaPt(II) or CisPt(II)) (1.5 μM) or with their platinum(IV) analogues (i.e., OxaPt(IV) or CisPt(IV)) (1.5 μM) for different time periods, ranging from 0.5 to 24 h prior to transfection. BCL-2 mRNA levels were quantified by NanoDrop and the data are presented as relative to that of untreated cells, which served as the negative control (NC) treatment. Data are depicted as mean values ± SEM with n = 3 samples per condition; note, 3 experimental replicates were similarly conducted for each cell line and treatment, yielding analogous results. Significance is defined as $^{**}p < 0.01$; $^{***}p < 0.001$.

chemically inert platinum(IV) prodrugs to circumvent these limitations.

Nanoparticle Characterization. There are many examples of utilizing nanoparticles for the delivery of siRNA along with different anticancer agents.[50−53] Whereas several studies have attempted nanoparticle incorporation of both siRNA and CisPt(II),[54−56] the results presented here reveal the advantages of utilizing a platinum(IV) agent to prevent siRNA platination and premature inactivation. To date, however, there have been only a few examples that utilize this latter approach.[57−59] Further investigations were, therefore, necessary to identify the optimal strategy by which to combine RNAi and platinum(IV) species to maximize their individual activities and to harness their synergy. Accordingly, we devised a transfection reagent capable of intracellular delivery of both platinum(IV) prodrugs and siRNA. For this work, we chose mPEG-*b*-PCL-*b*-PLL (P), which self-assembled into biodegradable micelles with a hydrophobic PCL core and a corona consisting of hydrophilic mPEG and positively charged PLL segments (M(P), where "M" stands for micelles; Scheme 1B). OxaPt(IV) was coupled to the PLL polymer through formation of an amide bond between the carboxyl group of its axial ligand and the free amino group of lysine, forming micelles that contained OxaPt(IV) (M(OxaPt(IV)). Similarly, siRNA was complexed with unreacted PLL chains through electrostatic interactions, forming micelles that contained BCL-2 (M(BCL-2)) or c-siRNA (M(c-siRNA)) (Scheme S3). Both OxaPt(IV) and siRNA species were also combined in a single micellar construct (M(OxaPt(IV)/BCL-2) or M(OxaPt(IV)/c-siRNA), respectively), consisting of a hydrophilic mPEG corona, a middle layer comprised of PLL/siRNA, and a hydrophobic core of PCL and PLL-OxaPt(IV) conjugates. When coincorporated within a single micelle, the siRNA was protected from interacting with the platinum species both by physical separation in different layers of the nanocomplex as well as by utilization of an unreactive platinum(IV) analogue (e.g., OxaPt(IV)). Each of these micellar constructs was generated to examine its relative ability to protect siRNA from platination, thereby preserving the effectiveness of RNAi. When taken up into cancer cells, the Pt in M(Oxa(IV)) rapidly reacted with intracellular reducing agents, including glutathione and ascorbic acid, liberating free OxaPt(II) that was capable of binding nuclear DNA (Scheme 1C).

M(P) had a mean diameter of 70.8 ± 0.5 nm, as determined by DLS, and a zeta potential of +46.1 ± 4.2 mV (Figure S19 and Table S2). To generate M(OxaPt(IV)), OxaPt(IV) was allowed to react with P at an initial molar ratio of 0.6:1 Pt to NH_2 groups (on the PLL block). Once coupled to PLL, the OxaPt(IV) conjugate became less water-soluble, driving its segregation within the PCL core and leaving unreacted PLL chains in the outer layer of M(OxaPt(IV)). This assertion is supported by experimental evidence that demonstrated a decrease in the CMC from 37.2 to 24 μg/mL (Figure S20), an increase in the mean particle diameter to 92.6 ± 2.6 nm (DLS), and a reduction in the zeta potential to +34.8 ± 1.9 for M(OxaPt(IV)) as compared to M(P) (Table S2). Overall, M(OxaPt(IV)) was comprised of 10 wt % Pt (by GFAAS), corresponding to a final OxaPt(IV) content of 20.4 wt %. This degree of loading was expected to yield 72% unreacted amino groups on the PLL corona of M(OxaPt(IV)), which were available for additional complexation of siRNA through electrostatic interactions.

To prove that M(OxaPt(IV)) was able to complex with BCL-2 siRNA, agarose gel electrophoresis experiments were conducted on siRNA after coincubation with either M(P) or M(OxaPt(IV)) (Figure S21A and S21B). The results showed that the mobility of the siRNA was completely inhibited when electrostatically complexed with M(P) above a ratio of nitrogen atoms in the PLL block of the polymer to phosphate units of the siRNA (N/P) that was greater than 2. Additionally, the mobility of the siRNA was reduced when complexed with M(OxaPt(IV)) above an N/P ratio of 4. By using Alexa488-labeled BCL-2 siRNA, the loading efficiency was determined to

DOI: 10.1021/jacs.6b12108
J. Am. Chem. Soc. 2017, 139, 3033−3044

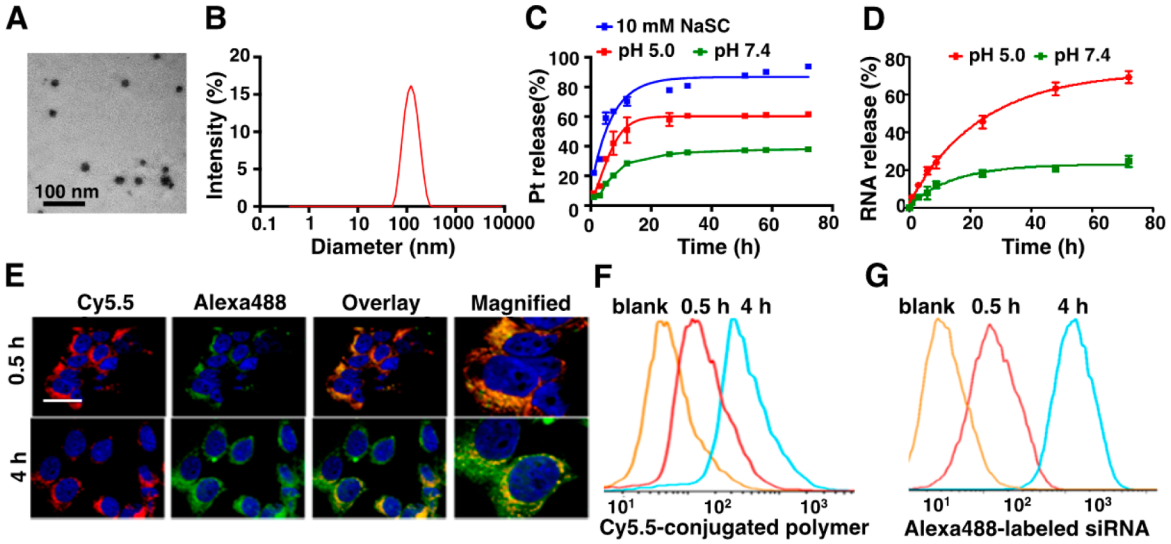

Figure 3. Micelles that covalently conjugate OxaPt(IV) and that are electrostatically complexed with BCL-2 siRNA demonstrate controlled release of both species. (A) TEM and (B) DLS results depicting the average size distributions for M(OxaPt(IV)/BCL-2) that were formed at an amine (per monomer unit, N) to phosphate (per nucleic acid, P) ratio (N/P ratio) of 8. The resultant micelles had a mean particle diameter of 78.9 ± 10.4 nm by TEM and 104.9 ± 2.1 nm by DLS. (C) Rapid in situ release of free OxaPt(II) was observed in high reducing environments (10 mM sodium ascorbate, NaSC) as compared to under physiologic (pH 7.4) or acidic (pH 5.0) in situ conditions. Individual data points are expressed as mean values ± SD for an $n = 3$ technical replicates per condition. A statistically significant separation in the curves was observed at all time points after 12 h ($p < 0.05$ via ANOVA). (D) The release of Alexa488-labeled siRNA from M(OxaPt(IV)/Alexa488 siRNA) was enhanced in low pH environments (pH 5.0 vs pH 7.4). Individual data points are again expressed as mean values ± SD for an $n = 3$ technical replicates per condition. A statistically significant separation in the curves was observed at all time points after 1 h ($p < 0.05$ via two-tailed t test). (E) Confocal laser scanning microscopy images were taken to visualize cellular uptake and cytoplasmic delivery of M(Cy5.5/Alexa488 siRNA/OxaPt(IV)). Images were obtained at 30 min (upper panel) and at 4 h (lower panel) after the addition of micelles to the MCF-7 cells. Note, cell nuclei were stained with DAPI (blue); Cy5.5-conjugated mPEG-*b*-PCL-*b*-PLL polymer (red) and Alexa488-labeled BCL-2 siRNA (green) were utilized to simultaneously and independently track the polymer and RNAi species, respectively (scale bar = 20 μm). Flow cytometry was employed to quantify the relative uptake of (F) Cy5.5-conjugated polymer and (G) Alexa488-labeled BCL-2 siRNA at various time points after the addition of M(Cy5.5/Alexa488 siRNA/OxaPt(IV)) to MCF-7 cells. Signals generated from the untreated (blank) cells are included for reference.

be approximately 99%; and, the final micelle composition consisted of 30% siRNA by weight (Figure S21C–E). Representative micelles, containing both BCL-2 siRNA and OxaPt(IV) formed at an N/P ratio of 8 (i.e., M(OxaPt(IV)/BCL-2)), were spherical with a mean particle diameter of 78.9 ± 10.4 nm and hydrodynamic size of 104.9 ± 2.1 nm, as determined by TEM and DLS, respectively (Figure 3A and 3B). M(OxaPt(IV)/BCL-2) had a reduced zeta potential of +26.6 ± 1.5 mV as compared to either M(P) or M(OxaPt(IV)) (Table S2), further supporting the shielding of free amines on the PLL corona of the micelles by siRNA. BCL-2 siRNA was also directly complexed to M(P) to generate M(BCL-2) with a mean particle diameter of 55.4 ± 0.7 nm (DLS) and a zeta potential of +35.5 ± 0.6 mV (Table S2). M(OxaPt(IV)/BCL-2) rapidly released OxaPt(II) under high reducing conditions in situ (Figure 3C), modeling the intracellular environment of tumor cells. However, it exhibited a slower and pH-dependent release of Alexa488-labeled siRNA (Figure 3D). Together, these data support a mechanism of rapid release of free OxaPt(II) followed by controlled release of siRNA after the intracellular uptake of M(OxaPt(IV)/BCL-2).

Cellular Uptake of Micelles. In order to determine the optimal conditions for siRNA delivery, we next used different concentrations of Luciferase GL3 and BCL-2 siRNA to achieve mRNA knockdown of their respective targets in a LUC$^+$ MCF-7 cell line. For both M(P) and M(OxaPt(IV)), an N/P ratio of 8 was employed for siRNA complexation. For effective RNAi of luciferase expression, 100 nM of Luciferase GL3 siRNA had to be utilized with either micellar construct (Figure S22). Although this was a higher concentration value for siRNA than was required with the commercially available RNAiMAX transfection kit (typically 1–2 nM), it was within the range of siRNA concentrations that have been utilized with other polymer-based transfection reagents.[60−62] To better study the kinetics and the mechanisms of micelle uptake and in vitro siRNA release, a Cy5.5-conjugated mPEG-*b*-PCL-*b*-PLL polymer was synthesized (Scheme S4). Alexa488-labeled siRNA was then complexed to micelles formed from this Cy5.5-conjugated polymer, generating M(Cy5.5/Alexa488 siRNA). OxaPt(IV) was also chemically bound to the Cy5.5-conjugated polymer to yield dual fluorophore-labeled micelles (i.e., M(Cy5.5/Alexa488 siRNA/OxaPt(IV))), which enabled simultaneous but independent in vitro tracking of both polymer and siRNA species (Scheme S5). MCF-7 cells were subsequently incubated with M(Cy5.5/Alexa488 siRNA/OxaPt(IV)) either for 30 min or for 4 h and were visualized by confocal laser scanning microscopy (Figure 3E). After 30 min of incubation, there was a colocalization of Cy5.5 (red) and Alexa488 fluorescence (green) in a punctate distribution within cells (depicted in orange within the magnified overlay image), consistent with the intracellular localization of intact micelles within endosomes. After 4 h, however, Alexa488 emission extended beyond the areas of corresponding Cy5.5 fluorescence and was apparent throughout the cytoplasm. Flow cytometry was used to quantify the relative intracellular levels of Cy5.5-labeled polymer and Alexa488-labeled siRNA both in MCF-7 (Figure 3F and 3G) and in OVCAR4 cells over time (Figure S23). Notably, cells that were treated with either M(Cy5.5/

DOI: 10.1021/jacs.6b12108
J. Am. Chem. Soc. 2017, 139, 3033−3044

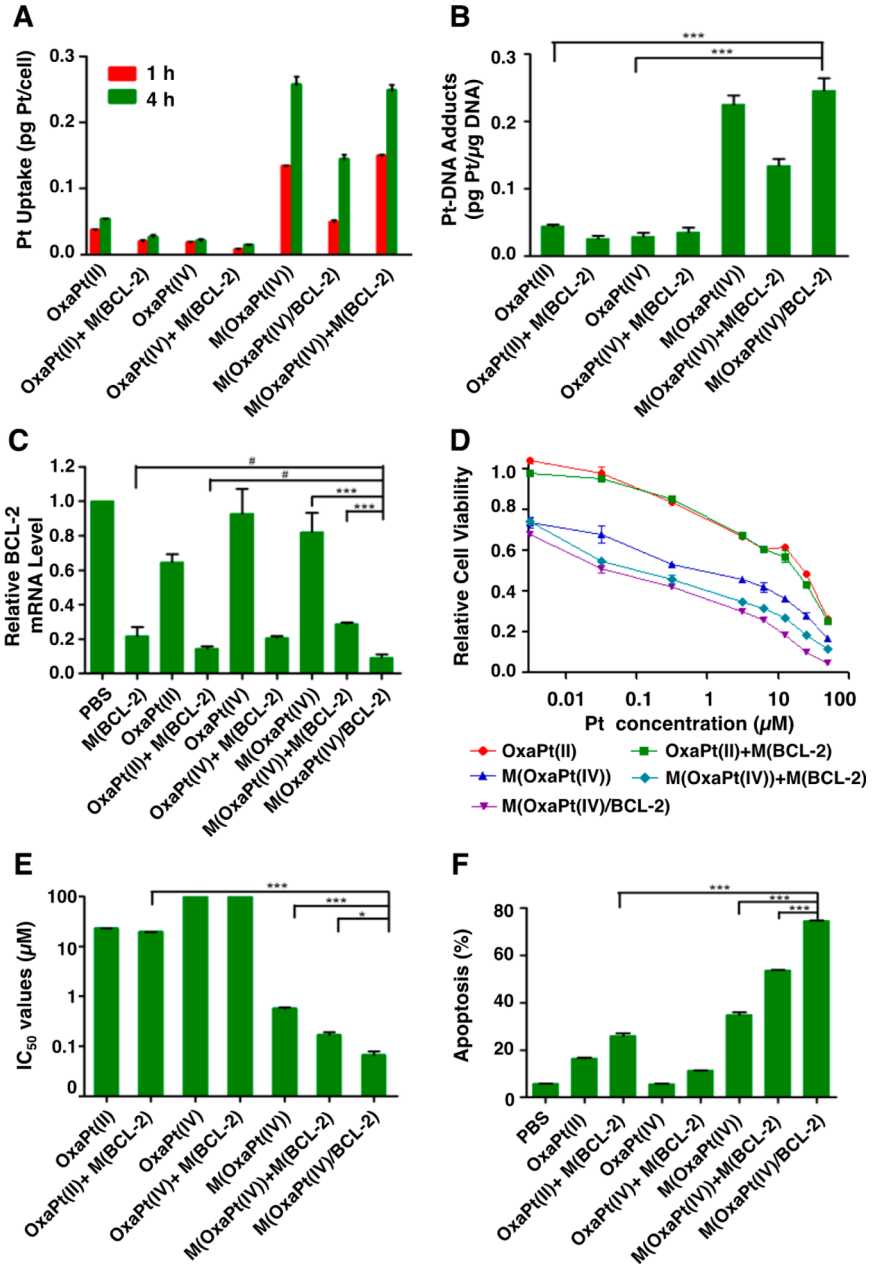

Figure 4. Coencapsulation of OxaPt(IV) and BCL-2 siRNA within a single micellar transfection reagent (i.e., M(OxaPt(IV)/BCL-2)) quantitatively maximizes the intracellular uptake of Pt, the numbers of Pt-DNA adducts that are formed, the suppression of BCL-2 mRNA levels, and the cytotoxicity to MCF-7 cells through augmentation of cellular apoptosis. (A) Pt uptake into MCF-7 cells after 1 h (red) and 4 h (green) of cellular exposure to various treatments as determined by ICP-MS. Equal concentrations of Pt (10 μM) and/or BCL-2 siRNA (100 nM) were used in each group and were respresentative of the concentrations of each species that are typically employed for in vitro cytotoxicity and RNAi experiments, respectively. (B) Total numbers of Pt-DNA adducts as assessed after 24 h of incubation with each experimental group. DNA was isolated after cellular lysis and the content of DNA-bound Pt was determined by ICP-MS. (C) Relative BCL-2 mRNA levels as determined by RT-qPCR conducted at 48 h after treatment with each experimental group. (D) Dose dependent cell viability plots and (E) IC_{50} values for cellular toxicity as determined by the MTT cellular viability assay, which was performed at 72 h after incubation with each experimental group. Experiments in A–D were performed in triplicate. IC_{50} values were derived from three independent experiments that each had three technical replicates per condition. Data are displayed as the mean values ± the standard deviation of the mean. (F) Total percentages of MCF-7 cells that underwent apoptosis as determined by flow cytometry at 36 h after treatment with various experimental groups. Equivalent concentrations of Pt (10 μM) ± BCL-2 siRNA (100 nM) were used for each condition. Data are depicted as mean values ± SEM with $n = 3$ samples per condition. In all cases, significance is defined as $^*p < 0.05$, $^{**}p < 0.01$, and $^{***}p < 0.001$. # denotes $p > 0.05$.

Alexa488 siRNA) or M(Cy5.5/Alexa488 siRNA/OxaPt(IV)) exhibited a 10-fold increase in Cy5.5-conjugated polymer and 40-fold increase in Alexa488-labeled siRNA after 4 h (Figure 3F), supporting active intracellular uptake of each species. Utilization of different small molecule inhibitors implicated multiple cellular uptake pathways but with a predominance of clathrin-dependent endocytosis (Figure S24). Together these results support a mechanism of active endocytosis of Cy5.5-conjugated micelles, rapid conversion of M(OxaPt(IV)) to free OxaPt(II)), and a slower cytoplasmic redistribution of

DOI: 10.1021/jacs.6b12108
J. Am. Chem. Soc. 2017, 139, 3033–3044

Table 2. Summary of IC_{50} Values (μM) for MCF-7, OVCAR4, A2780 and A2780DDP Cells Treated with Various Combinations of Platinum-Containing Anticancer Agents and/or siRNA Species

Treatment Groups	MCF-7	OVCAR4	A2780	A2780DDP
OxaPt(II)	23.05 ± 0.25	15.45 ± 0.50	2.90 ± 0.28	18.80 ± 0.99
OxaPt(II) + M(c-siRNA)	28.51 ± 0.34	21.60 ± 0.71	3.75 ± 0.91	22.25 ± 1.63
OxaPt(II) + M(BCL-2)	19.20 ± 0.42	9.24 ± 1.50	1.60 ± 0.14	10.55 ± 1.34
OxaPt(IV)	>100	>100	15.85 ± 2.76	>100
OxaPt(IV) + M(c-siRNA)	>100	>100	12.65 ± 1.20	>100
OxaPt(IV) + M(BCL-2)	>100	>100	8.60 ± 1.13	>100
M(OxaPt(IV))	0.54 ± 0.03	1.79 ± 0.10	0.87 ± 0.13	1.45 ± 0.07
M(OxaPt(IV)) + M(c-siRNA)	0.43 ± 0.01	1.37 ± 0.12	0.72 ± 0.09	1.06 ± 0.20
M(OxaPt(IV)) + M(BCL-2)	0.17 ± 0.02	0.43 ± 0.01	0.51 ± 0.03	0.60 ± 0.08
M(OxaPt(IV)/c-siRNA)	0.43 ± 0.02	1.80 ± 0.25	0.59 ± 0.06	0.72 ± 0.05
M(OxaPt(IV)/BCL-2)	0.06 ± 0.01	0.12 ± 0.01	0.39 ± 0.02	0.42 ± 0.08

Alexa488-labeled siRNA, which was consistent with controlled release and endosomal escape. This relative temporal and spatial separation between OxaPt(II) and siRNA release was expected to limit the formation of intracellular Pt-siRNA adducts and to promote the individual and synergistic activities of these otherwise reactive species.

Optimum Strategy for Combining RNAi and Platinum-Based Anticancer Agents. After having validated effective intracellular delivery with our transfection reagent, we next compared various strategies for combining BCL-2 siRNA and platinum-based anticancer agents in order to achieve maximal synergistic activity. For all siRNA-containing groups, the concentration of siRNA (100 nM) was kept constant and was transfected using various polymeric micelles formed at an N/P ratio of 8. These micelles had no inherent effects on cellular viability in the absence of the platinum-based species (Figure S25). We next conducted a series of experiments in which MCF-7 cells were treated with increasing concentrations of different platinum formulations (i.e., free OxaPt(II), free OxaPt(IV), or M(OxaPt(IV))), either individually or in combination with M(BCL-2) or M(c-siRNA). Cells were also treated with siRNA and platinum-based species that were codelivered via a single micellar construct (i.e., M(OxaPt(IV)/BCL-2) or M(OxaPt(IV)/c-siRNA)). In all cases, BCL-2 mRNA levels were measured by RT-qPCR, intracellular Pt concentrations and the numbers of Pt-DNA adducts were quantified by ICP-MS, and cellular viability was determined by the colorimetric MTT assay after each treatment.

Decreased amounts of intracellular Pt were detected after both 1 and 4 h of exposure to free OxaPt(IV) as compared to free OxaPt(II) (Figure 4A and Table S3). Intracellular Pt levels were markedly enhanced (by ~3−8 fold) when treated with M(OxaPt(IV)) as opposed to various free drug formulations of either OxaPt(II) or OxaPt(IV) that were administered at identical Pt concentrations. The intracellular levels of Pt also increased 2-fold between 1 and 4 h after administration of M(OxaPt(IV)), which, again, supported a time-dependent mechanism of micelle uptake via active endocytosis.

Coadministration of M(OxaPt(IV)) and a separate micellar construct containing only siRNA (e.g., M(BCL-2)), however, resulted in a relative 2-fold decrease in the intracellular content of Pt as compared to cells that were treated with either M(OxaPt(IV)) alone or M(OxaPt(IV)/BCL-2) at equivalent Pt concentrations. These results indicate that micelle uptake via endocytosis was not only time-dependent but also saturable. These observations were further supported by analogous measurements of the numbers of intracellular Pt-DNA adducts that could be detected after 24 h of treatment (Figure 4B and Table S3). A markedly enhanced number of Pt-DNA adducts (~10 fold increase) were measured after treatment with M(OxaPt(IV)) as opposed to either free OxaPt(II) or free OxaPt(IV) administered at equivalent Pt concentrations and for similar incubation periods. Coadministration of two separate micellar constructs of M(OxaPt(IV)) and M(BCL-2) resulted in the generation of half the numbers of Pt-DNA adducts as compared to treatment with M(OxaPt(IV)) alone or with M(OxaPt(IV)/BCL-2), which, again, supported a saturable limit for micelle uptake by MCF-7 cells. To promote the highest intracellular levels of Pt and the maximal numbers of Pt-DNA adducts, combined delivery of OxaPt(IV) and BCL-2 siRNA via a single micellar construct was found to be optimal.

Thereafter, we examined the relative levels of BCL-2 mRNA within cells after treatment with each experimental group (Figure 4C and S26). Whereas free OxaPt(II) decreased BCL-2 mRNA levels to 65% that of untreated (control) cells, consistent with its known pro-apoptotic activity,[63] effective mRNA suppression was only achieved with BCL-2 siRNA treatment (i.e., suppression to less than 30% of baseline mRNA levels). Coadministration of free OxaPt(II), free OxaPt(IV), or M(OxaPt(IV)) together with M(BCL-2) did not further inhibit mRNA levels beyond that which was obtained with M(BCL-2) treatment alone. These results indicate that when siRNA was electrostatically complexed with polymeric micelles prior to platinum(II) exposure, it was effectively protected from platination. Notably, coincorporation of BCL-2 siRNA and OxaPt(IV) in the same micellar construct (i.e., M(OxaPt(IV)/BCL-2)) did achieve a statistically significant improvement in BCL-2 mRNA suppression (to less than 10% of baseline levels). As such, delivery of BCL-2 siRNA and OxaPt(IV) with a single micelle not only ensured siRNA transcript stability but also promoted maximal suppression of mRNA levels beyond that which was achievable with either agent only or when they were combined by alternative means.

Ultimately, the goals of combining RNAi with platinum-based therapies are to explore changes in treatment responses and biological activities that are mediated by the suppression of specific gene products. We, therefore, interrogated changes in the in vitro viability of MCF-7 cells that were treated with various experimental combinations of platinum-based species and BCL-2 siRNA. We measured changes in cellular viability as a function of increasing quantities of free OxaPt(II), free OxaPt(IV), or M(OxaPt(IV)), either as single treatments or in combinations with either M(BCL-2) or M(c-siRNA) (Figure 4D and S27). Cells were also treated with M(OxaPt(IV)/BCL-

DOI: 10.1021/jacs.6b12108
J. Am. Chem. Soc. 2017, 139, 3033−3044

2) or M(OxaPt(IV)/c-siRNA) at equivalent Pt concentrations for comparative purposes. Synergistic treatment responses from any combination of platinum-based species and siRNA were defined as a decrease in the IC_{50} value as compared to cells that were exposed to the same platinum-based therapy alone. Although the combination of free OxaPt(IV) with M(BCL-2) did show a synergistic treatment effect, which was not obvious in the combination of free OxaPt(II) and M(BCL-2), free OxaPt(IV)-containing treatments were approximately 10-fold less potent than free OxaPt(II) at inducing cellular toxicity (Figure 4E). By comparison, M(OxaPt(IV)) was 100× more potent than free OxaPt(IV) and displayed 10-fold greater cytotoxicity than free OxaPt(II). Whereas the combination of M(BCL-2) and M(OxaPt(IV)) did result in a statistically significant improvement in antiproliferative activity, M(OxaPt-(IV)/BCL-2) displayed the highest in vitro potency, yielding an IC_{50} value of 60 nM as compared to 23 ±0.25 μM for free OxaPt(II) alone. This dramatically enhanced efficacy for M(OxaPt(IV)/BCL-2) was further corroborated by testing each of the various treatment combinations on additional cell lines (i.e., OVCAR4, A2780 and A2780DDP; Table 2). To investigate the biological mechanisms underlying this improved activity, we performed flow cytometry to quantify the populations of MCF-7 cells that were apoptotic after 36 h of exposure to each experimental group (Figure 4F and S28). When compared to treatment with free OxaPt(II) (at equivalent Pt concentrations and for identical durations of time), treatment with M(OxaPt(IV)/BCL-2) resulted in a 4-fold increase in the total number of cells that had underwent apoptosis. Notably, this level of pro-apoptotic activity was twice that of M(OxaPt(IV)) alone and 1.5-fold greater than that of the combination of M(OxaPt(IV)) and M(BCL-2). These experiments confirmed that the delivery of BCL-2 siRNA and OxaPt(IV) via a single micellar construct resulted in the highest numbers of apoptotic events as compared to all other strategies for combining BCL-2 siRNA with different platinum-based species.

CONCLUSIONS

RNAi approaches are extensively used to study molecular responses that mediate acquired cellular resistance to platinum-containing regimens. The success of these endeavors relies on the preserved activity of the exogenous RNAi transcript when combined with platinum-based anticancer agents. Here, we demonstrated rapid and extensive Pt-siRNA adduct formation when siRNA was incubated with platinum(II)-based agents at concentrations and for time intervals that are typically used for in vitro RNAi experiments. Notably, siRNA was protected from inactivation by combining it with a platinum(IV) analogue, but this combination resulted in reduced cytotoxicity as compared to using the active platinum(II) agent alone. In order to promote effective RNAi and to maximize the individual and synergistic activities of siRNA and platinum-based anticancer agents, we found that both species had to be coincorporated within a single micelle-based delivery vehicle. A generalized adoption of this strategy may lead to the development of novel therapeutics and may be used to identify drug targets that would otherwise be missed in conventional screens that typically combine RNAi with platinum(II)-based anticancer agents.

ASSOCIATED CONTENT

Supporting Information

The Supporting Information is available free of charge on the ACS Publications website at DOI: 10.1021/jacs.6b12108.

Supplemental Materials and Methods, Schemes S1−S5, Figures S1−S28, and Tables S1−S3 (PDF)

AUTHOR INFORMATION

Corresponding Author

*ppg@mit.edu

ORCID

P. Peter Ghoroghchian: 0000-0002-2564-1950

Notes

The authors declare no competing financial interest.

ACKNOWLEDGMENTS

The authors would like to acknowledge Professor Stephen J. Lippard for helpful discussions. PPG acknowledges support from the Kathryn Fox Samway Foundation. Research support was also provided from the Flow Cytometry, Microscopy, and Nanomaterials Core Facilities in the Swanson Biotechnology Center of the Koch Institute at MIT. This research was funded by the Charles W. and Jennifer C. Johnson Clinical Investigator Fund from the Koch Institute at MIT as well as by a 2015 Amgen Research Grant from the Foundation for Women's Cancer.

REFERENCES

(1) Rosenberg, B.; Vancamp, L.; Trosko, J. E.; Mansour, V. H. *Nature* **1969**, *222*, 385.
(2) Alderden, R. A.; Hall, M. D.; Hambley, T. W. *J. Chem. Educ.* **2006**, *83*, 728.
(3) Fennell, D. A.; Summers, Y.; Cadranel, J.; Benepal, T.; Christoph, D. C.; Lal, R.; Das, M.; Maxwell, F.; Visseren-Grul, C.; Ferry, D. *Cancer Treat. Rev.* **2016**, *44*, 42.
(4) Ho, G. Y.; Woodward, N.; Coward, J. I. G. *Crit Rev. Oncol Hematol* **2016**, *102*, 37.
(5) Agarwal, R.; Kaye, S. B. *Nat. Rev. Cancer* **2003**, *3*, 502.
(6) Stordal, B.; Pavlakis, N.; Davey, R. *Cancer Treat. Rev.* **2007**, *33*, 688.
(7) Shen, D.-W.; Pouliot, L. M.; Hall, M. D.; Gottesman, M. M. *Pharmacol. Rev.* **2012**, *64*, 706.
(8) Chien, J.; Kuang, R.; Landen, C.; Shridhar, V. *Front. Oncol.* **2013**, *3*, 251.
(9) Davis, A.; Tinker, A. V.; Friedlander, M. *Gynecol. Oncol.* **2014**, *133*, 624.
(10) O'Grady, S.; Finn, S. P.; Cuffe, S.; Richard, D. J.; O'Byrne, K. J.; Barr, M. P. *Cancer Treat. Rev.* **2014**, *40*, 1161.
(11) Konstantinopoulos, P. A.; Ceccaldi, R.; Shapiro, G. I.; D'Andrea, A. D. *Cancer Discovery* **2015**, *5*, 1137.
(12) Bartz, S. R.; Zhang, Z.; Burchard, J.; Imakura, M.; Martin, M.; Palmieri, A.; Needham, R.; Guo, J.; Gordon, M.; Chung, N.; Warrener, P.; Jackson, A. L.; Carleton, M.; Oatley, M.; Locco, L.; Santini, F.; Smith, T.; Kunapuli, P.; Ferrer, M.; Strulovici, B.; Friend, S. H.; Linsley, P. S. *Mol. Cell. Biol.* **2006**, *26*, 9377.
(13) Arora, S.; Bisanz, K. M.; Peralta, L. A.; Basu, G. D.; Choudhary, A.; Tibes, R.; Azorsa, D. O. *Gynecol. Oncol.* **2010**, *118*, 220.
(14) Diehl, P.; Tedesco, D.; Chenchik, A. *Drug Discovery Today: Technol.* **2014**, *11*, 11.
(15) Mackay, C.; Carroll, E.; Ibrahim, A. F. M.; Garg, A.; Inman, G. J.; Hay, R. T.; Alpi, A. F. *Cancer Res.* **2014**, *74*, 2246.
(16) Leung, A. W. Y.; Dragowska, W. H.; Ricaurte, D.; Kwok, B.; Mathew, V.; Roosendaal, J.; Ahluwalia, A.; Warburton, C.; Laskin, J. J.; Stirling, P. C.; Qadir, M. A.; Bally, M. B. *Oncotarget* **2015**, *6*, 17161.

DOI: 10.1021/jacs.6b12108
J. Am. Chem. Soc. 2017, 139, 3033−3044

(17) Kwok, J. M. M.; Peck, B.; Monteiro, L. J.; Schwenen, H. D. C.; Millour, J.; Coombes, R. C.; Myatt, S. S.; Lam, E. W. F. *Mol. Cancer Res.* **2010**, *8*, 24.
(18) McAuliffe, S. M.; Morgan, S. L.; Wyant, G. A.; Tran, L. T.; Muto, K. W.; Chen, Y. S.; Chin, K. T.; Partridge, J. C.; Poole, B. B.; Cheng, K.-H.; Daggett, J.; Cullen, K.; Kantoff, E.; Hasselbatt, K.; Berkowitz, J.; Muto, M. G.; Berkowitz, R. S.; Aster, J. C.; Matulonis, U. A.; Dinulescu, D. M. *Proc. Natl. Acad. Sci. U. S. A.* **2012**, *109*, E2939.
(19) Moreno-Smith, M.; Halder, J. B.; Meltzer, P. S.; Gonda, T. A.; Mangala, L. S.; Rupaimoole, R.; Lu, C.; Nagaraja, A. S.; Gharpure, K. M.; Kang, Y.; Rodriguez-Aguayo, C.; Vivas-Mejia, P. E.; Zand, B.; Schmandt, R.; Wang, H.; Langley, R. R.; Jennings, N. B.; Ivan, C.; Coffin, J. E.; Armaiz, G. N.; Bottsford-Miller, J.; Kim, S. B.; Halleck, M. S.; Hendrix, M. J. C.; Bornman, W.; Bar-Eli, M.; Lee, J.-S.; Siddik, Z. H.; Lopez-Berestein, G.; Sood, A. K. *J. Clin. Invest.* **2013**, *123*, 2119.
(20) Xue, W.; Dahlman, J. E.; Tammela, T.; Khan, O. F.; Sood, S.; Dave, A.; Cai, W.; Chirino, L. M.; Yang, G. R.; Bronson, R.; Crowley, D. G.; Sahay, G.; Schroeder, A.; Langer, R.; Anderson, D. G.; Jacks, T. *Proc. Natl. Acad. Sci. U. S. A.* **2014**, *111*, E3553.
(21) Reyes-González, J. M.; Armaiz-Peña, G. N.; Mangala, L. S.; Valiyeva, F.; Ivan, C.; Pradeep, S.; Echevarría-Vargas, I. M.; Rivera-Reyes, A.; Sood, A. K.; Vivas-Mejía, P. E. *Mol. Cancer Ther.* **2015**, *14*, 2260.
(22) Nascimento, A. V.; Gattacceca, F.; Singh, A.; Bousbaa, H.; Ferreira, D.; Sarmento, B.; Amiji, M. M. *Nanomedicine (London, U. K.)* **2016**, *11*, 767.
(23) Rana, T. M. *Nat. Rev. Mol. Cell Biol.* **2007**, *8*, 23.
(24) Dykxhoorn, D. M.; Novina, C. D.; Sharp, P. A. *Nat. Rev. Mol. Cell Biol.* **2003**, *4*, 457.
(25) Jamieson, E. R.; Lippard, S. J. *Chem. Rev.* **1999**, *99*, 2467.
(26) Reedijk, J. *Chem. Rev.* **1999**, *99*, 2499.
(27) Baik, M.-H.; Friesner, R. A.; Lippard, S. J. *J. Am. Chem. Soc.* **2003**, *125*, 14082.
(28) Fichtinger-Schepman, A. M.; van der Veer, J. L.; den Hartog, J. H.; Lohman, P. H.; Reedijk, J. *Biochemistry* **1985**, *24*, 707.
(29) Sorenson, C. M.; Barry, M. A.; Eastman, A. *J. Natl. Cancer Inst* **1990**, *82*, 749.
(30) Gonzalez, V. M.; Fuertes, M. A.; Alonso, C.; Perez, J. M. *Mol. Pharmacol.* **2001**, *59*, 657.
(31) Gatti, L.; Supino, R.; Perego, P.; Pavesi, R.; Caserini, C.; Carenini, N.; Righetti, S. C.; Zuco, V.; Zunino, F. *Cell Death Differ.* **2002**, *9*, 1352.
(32) Qin, L. F.; Ng, I. O. L. *Cancer Lett.* **2002**, *175*, 27.
(33) (a) Hostetter, A. A.; Chapman, E. G.; DeRose, V. J. *J. Am. Chem. Soc.* **2009**, *131*, 9250. (b) Osborn, M. F.; White, J. D.; Haley, M. M.; DeRose, V. J. *ACS Chem. Biol.* **2014**, *9*, 2404. (c) Alberti, E.; Zampakou, M.; Donghi, D. *J. Inorg. Biochem.* **2016**, *163*, 278.
(34) Chapman, E. G.; DeRose, V. J. *J. Am. Chem. Soc.* **2010**, *132*, 1946.
(35) Hostetter, A. A.; Osborn, M. F.; DeRose, V. J. *ACS Chem. Biol.* **2012**, *7*, 218.
(36) Hedman, H. K.; Kirpekar, F.; Elmroth, S. K. C. *J. Am. Chem. Soc.* **2011**, *133*, 11977.
(37) (a) Polonyi, C.; Elmroth, S. K. C. *Dalton Trans* **2013**, *42*, 14959. (b) Polonyi, C.; Alshiekh, A.; Sarsam, L. A.; Clausén, M.; Elmroth, S. K. C. *Dalton Trans* **2014**, *43*, 11941.
(38) Xiao, H.; Qi, R.; Liu, S.; Hu, X.; Duan, T.; Zheng, Y.; Huang, Y.; Jing, X. *Biomaterials* **2011**, *32*, 7732.
(39) Xiao, H.; Song, H.; Yang, Q.; Cai, H.; Qi, R.; Yan, L.; Liu, S.; Zheng, Y.; Huang, Y.; Liu, T.; Jing, X. *Biomaterials* **2012**, *33*, 6507.
(40) Zheng, Y.-R.; Suntharalingam, K.; Johnstone, T. C.; Yoo, H.; Lin, W.; Brooks, J. G.; Lippard, S. J. *J. Am. Chem. Soc.* **2014**, *136*, 8790.
(41) Reiber, H.; Ruff, M.; Uhr, M. *Clin. Chim. Acta* **1993**, *217*, 163.
(42) Jones, D. P.; Carlson, J. L.; Mody, V. C.; Cai, J.; Lynn, M. J.; Sternberg, P. *Free Radical Biol. Med.* **2000**, *28*, 625.
(43) Khorsand, B.; Lapointe, G.; Brett, C.; Oh, J. K. *Biomacromolecules* **2013**, *14*, 2103.
(44) Mikirova, N.; Casciari, J.; Riordan, N.; Hunninghake, R. *J. Transl. Med.* **2013**, *11*, 191.
(45) Zhang, A.; Zhang, Z.; Shi, F.; Xiao, C.; Ding, J.; Zhuang, X.; He, C.; Chen, L.; Chen, X. *Macromol. Biosci.* **2013**, *13*, 1249.
(46) Cho, H. J.; Kim, J. K.; Kim, K. D.; Yoon, H. K.; Cho, M.-Y.; Park, Y. P.; Jeon, J. H.; Lee, E. S.; Byun, S.-S.; Lim, H. M.; Song, E. Y.; Lim, J.-S.; Yoon, D.-Y.; Lee, H. G.; Choe, Y.-K. *Cancer Lett.* **2006**, *237*, 56.
(47) Qi, R.; Hu, X.; Yan, L.; Chen, X.; Huang, Y.; Jing, X. *J. Controlled Release* **2011**, *152* (Suppl 1), e167.
(48) Xiao, H.; Li, W.; Qi, R.; Yan, L.; Wang, R.; Liu, S.; Zheng, Y.; Xie, Z.; Huang, Y.; Jing, X. *J. Controlled Release* **2012**, *163*, 304.
(49) Goodwin, A. P.; Mynar, J. L.; Ma, Y.; Fleming, G. R.; Fréchet, J. M. J. *J. Am. Chem. Soc.* **2005**, *127*, 9952.
(50) Deng, Z. J.; Morton, S. W.; Ben-Akiva, E.; Dreaden, E. C.; Shopsowitz, K. E.; Hammond, P. T. *ACS Nano* **2013**, *7*, 9571.
(51) Gandhi, N. S.; Tekade, R. K.; Chougule, M. B. *J. Controlled Release* **2014**, *194*, 238.
(52) Saraswathy, M.; Gong, S. *Mater. Today* **2014**, *17*, 298.
(53) Jones, S. K.; Lizzio, V.; Merkel, O. M. *Biomacromolecules* **2016**, *17*, 76.
(54) Ganesh, S.; Iyer, A. K.; Weiler, J.; Morrissey, D. V.; Amiji, M. M. *Mol. Ther.–Nucleic Acids* **2013**, *2*, e110.
(55) Meng, H.; Mai, W. X.; Zhang, H.; Xue, M.; Xia, T.; Lin, S.; Wang, X.; Zhao, Y.; Ji, Z.; Zink, J. I.; Nel, A. E. *ACS Nano* **2013**, *7*, 994.
(56) Babu, A.; Wang, Q.; Muralidharan, R.; Shanker, M.; Munshi, A.; Ramesh, R. *Mol. Pharmaceutics* **2014**, *11*, 2720.
(57) Xu, X.; Xie, K.; Zhang, X.-Q.; Pridgen, E. M.; Park, G. Y.; Cui, D. S.; Shi, J.; Wu, J.; Kantoff, P. W.; Lippard, S. J.; Langer, R.; Walker, G. C.; Farokhzad, O. C. *Proc. Natl. Acad. Sci. U. S. A.* **2013**, *110*, 18638.
(58) Shen, S.; Sun, C.-Y.; Du, X.-J.; Li, H.-J.; Liu, Y.; Xia, J.-X.; Zhu, Y.-H.; Wang, J. *Biomaterials* **2015**, *70*, 71.
(59) Yu, H.; Guo, C.; Feng, B.; Liu, J.; Chen, X.; Wang, D.; Teng, L.; Li, Y.; Yin, Q.; Zhang, Z.; Li, Y. *Theranostics* **2016**, *6*, 14.
(60) Gabrielson, N. P.; Lu, H.; Yin, L.; Kim, K. H.; Cheng, J. *Mol. Ther.* **2012**, *20*, 1599.
(61) Kozielski, K. L.; Tzeng, S. Y.; Green, J. J. *WIREs Nanomed. Nanobiotechnol.* **2013**, *5*, 449.
(62) Sun, C.-Y.; Shen, S.; Xu, C.-F.; Li, H.-J.; Liu, Y.; Cao, Z.-T.; Yang, X.-Z.; Xia, J.-X.; Wang, J. *J. Am. Chem. Soc.* **2015**, *137*, 15217.
(63) Hayward, R. L.; Macpherson, J. S.; Cummings, J.; Monia, B. P.; Smyth, J. F.; Jodrell, D. I. *Mol. Cancer Ther.* **2004**, *3*, 169.

DOI: 10.1021/jacs.6b12108
J. Am. Chem. Soc. 2017, 139, 3033−3044